CEAS Space Journal
https://doi.org/10.1007/s12567-023-00531-x

ORIGINAL PAPER

Advancing spacecraft demisability through a novel composite bolt joint system: a step toward sustainable and safe space environments

Alexandre A. Looten[1] · Albert Vodermayer[2] · Antonio Caiazzo[3] · Ralf Usinger[4] · Muriel Richard[5] · Véronique Michaud[1]

Received: 30 August 2023 / Revised: 6 November 2023 / Accepted: 9 November 2023

Abstract
From the recent awareness of the booming number of space debris and their derived worldwide re-entry event threat originating from the use of high survivability components, complementary mitigation measures must be taken for future orbital elements. In this direction, the implementation of a design for demise at an early stage of spacecraft conception allows a progressive and effective solution. As part of a collaborative effort launched by École Polytechnique Fédérale de Lausanne and the European Space Agency, we focus on the evaluation of polymer composite bolts as the main structural satellite panel fastening systems to improve the overall spacecraft demisability during its destructive re-entry into the atmosphere as compared to baseline critical systems, while maintaining equivalent mission-relevant properties. Two carbon fiber-reinforced polyetheretherketone (PEEK) designs were compared to a stainless steel baseline in terms of static properties at room temperature, dynamic properties over a temperature range, as well as demise capability by static re-entry simulation testing. The results led us to identify a promising short CF/PEEK composite bolt design.

Keywords Carbon fiber/PEEK · Composite fastener · Assembly · Demisability · Design for demise · Joint · Bolt

1 Introduction

Considering the thriving number of orbital launches and satellited objects since the beginning of 2023, showing a respective increase of 43% and 404% as compared to 2019 [1], concerns arise about the occupation of the confined LEO region. Moreover, as "*what goes up, must come down*", we impose a direct threat on ourselves and future generations knowing that most of these objects will start to fall back into the dense atmosphere within 25 years of mission completion. This issue stems from re-entry resistant spacecraft components in combination with an uncontrolled re-entry accidental event or selected post-mission disposal option, leading to a global Earth ground casualty risk. By pursuing the situation awareness and more particularly focusing on a design for demise (D4D) mitigation approach, sustainable disposal options can be assessed at an early stage in the space mission planning and thus facilitating its implementation.

During uncontrolled re-entry, the object's hypersonic speed leads to the formation of a frontal plasma shock wave, generating an intense radiative heating to the part surface. At material level, this aerothermal heating translates into rapid heating inducing surface temperature to rise to above a thousand degrees Celsius, generating complex decomposition behaviors depending on the material type. For metals, it causes surface oxidation, melting and up to vaporization. Whereas for the material of interest in this study, fiber-reinforced polymer composites, it exhibits a more complex degradation process. The polymer matrix quickly initiates pyrolysis leading to surface recession and char generation, then the exposed fibers, depending on the fiber type, either melt or start oxidizing with the char in the presence of atmospheric oxygen. These combined phenomena lead to by-products outgassing, spallation, and possibly

✉ Alexandre A. Looten
alexandre.looten@epfl.ch

[1] École Polytechnique Fédérale de Lausanne (EPFL), Institute of Materials (IMX), Laboratory for Processing of Advanced Composites (LPAC), Lausanne, Switzerland

[2] icotec ag, Altstätten, Switzerland

[3] European Space Agency (ESA-ESTEC), Noordwijk, The Netherlands

[4] Beyond Gravity Schweiz AG, Zurich, Switzerland

[5] ClearSpace SA, Renens, Switzerland

Published online: 14 December 2023

ply delamination if submitted to sufficient heat and\or aerodynamic forces.

Hence for this latter class of material, the demise capability is mainly driven by five temperature and heating rate-dependent materials parameters: melting temperature, specific heat capacity, heat of fusion/ablation, surface catalycity, and thermal conductivity [2, 3]. The material selection process is a key aspect of D4D with particular attention to the replacement of critical materials, defined as resistant to a typical re-entry environment such as iron-based alloys, titanium alloys, and in certain conditions carbon fiber-reinforced thermoset polymer (CFRP) [4], by demisable options such as aluminum alloys or natural fiber-reinforced polymer composites, as illustrated in Fig. 1, where flax fiber-reinforced composite demisability was evaluated for D4D applications [5].

Material research and innovation play a crucial role in the space industry since the beginning of the space-age. The implementation of novel materials has been proven to be game-changing on several conception levels; the switch from metallic alloys to high-performance composites of aircraft and spacecraft structures in the 1960s allowed a significant improvement of stiffness over mass design optimization. This is mainly based on the reinforced polymer composites' great versatility in terms of geometry, composition, and properties.

Our work focuses on D4D applied to satellite external panels. These components play a key role in the demisability phenomenology as they typically shade internal components during the first re-entry phase, thus delaying their exposure and so their disintegration from the destructive environment [2, 6]. The implementation of demisable sandwich panel skins and/or fastening systems could provide means to increase the exposure of internal components to favor early demise.

The research topic of demisable joining systems has gained attention relatively recently, with initial methods being introduced in 2016. For example, the OHB Design-for-Demise Breadboarding test campaign evaluated four different designs, a two part inserts with solder material, an adhesive bonded cleat, a composite insert, and a shape memory alloy cylinder bolt system [7]. The latter exhibited the most promising and clear separation at the expected triggering temperature. However, the composite insert made of carbon fiber-reinforced polyetheretherketone (CF/PEEK) did not show a distinct improvement when compared to a standard aluminum insert, in which joint failure occurred due to honeycomb-insert adhesive potting material degradation. Additional ongoing activities related to this topic include the development of a demisable low melting temperature washer mounted on a modified cleat specific from ThalesAlenia Space, made from a zinc-based alloy EZAC™ [8]. Furthermore, an innovative concept of demisable joint patches manufactured by additive manufacturing of CF/PEEK, containing fiber content up to 30%, has been evaluated by a team at DLR led by Sakraker-Ozmen and presented by Patzwald et al. [9].

The present article presents the substitution of critical through-thickness bolt and nut materials by a high-performance composite system made of CF/PEEK. This replacement should allow a much faster and earlier passive panel release, due to the matrix melting as opposed to degradation and charring in the case of thermoset matrices. This approach differs from the OHB composite embedded insert, as documented in reference [6], as in our case the exposure to the high-enthalpy flow is direct, enabling a dedicated and specific break-up mechanism of the composite part. Such setup is characterized by the rapid initiation of matrix melting, facilitated by the high-enthalpy conditions, and the application of aerodynamic shear forces. Consequently,

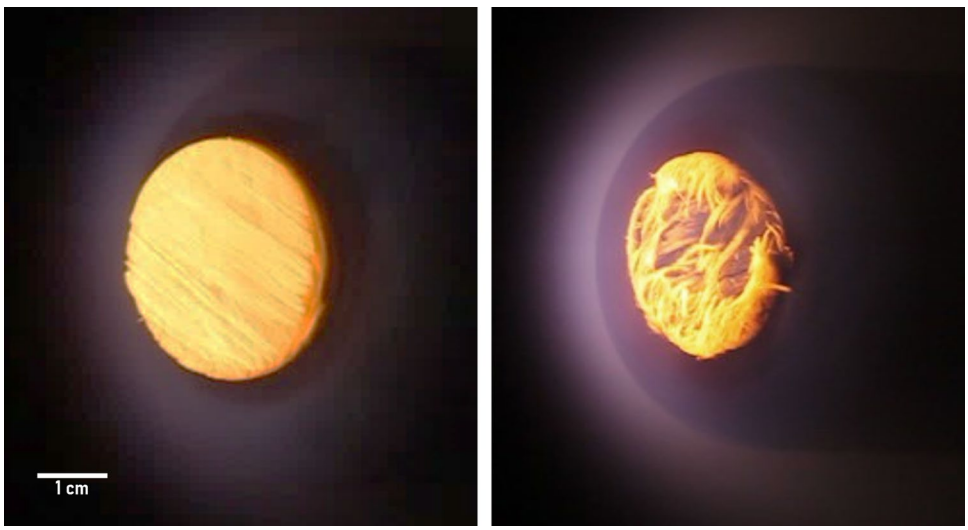

Fig. 1 Plasma wind tunnel sample demise evaluation of re-entry resistant carbon (left) vs demisable flax (right) fiber-reinforced polymer after 30 s under 925 kW/m^2 heat flux at IRS PWK4 facility

these factors synergistically encourage the intended separation of the assembly. In a manner similar to DLR's joint patches approach [9], our method also shares similarities, yet with reduced requirements for extensive structural analysis and integration steps due to the utilization of a conventional bolt joint system.

An overall higher spacecraft demisability, synonym of lower casualty risk, is thus expected following our latest results and previous studies, such as presented by Pagan et al. [5] and Patzwald et al. [9]. Such technology should be integrated in combination with demisable panels, preventing critical increase of the casualty area and risk by spreading additional potentially surviving fragments. Such step can be assessed with the Survival and Risk Analysis—SARA dedicated module of the Debris Risk Assessment and Mitigation Analysis—DRAMA tool through the re-entry demise analysis of the panels' separations and the induced risk.

Material level characterizations in addition to mechanical capability and demise evaluation testing have been performed to allow the process of such component integration in a space-qualified structure.

2 Materials

The selected CF/PEEK material ideally fits aerospace applications by its combination of both high-end mechanical performance carbon fibers and thermoplastic matrix. Compared to the aerospace grade Ti6Al4V titanium alloy, the resulting composite with a fiber volume content of at least 50% presents high specific ultimate tensile strength over density (respectively around 210 MPa/g cm^{-3} for the Ti alloy versus 180 MPa/g cm^{-3} for this composite), low thermal expansion coefficient (9 µm/m °C vs 2.5 µm/m °C) [10], in addition of high vacuum compatibility and high space environment resistance [11]. Regarding D4D applications, its relatively low melting temperature at 350 °C, as compared to structural metals is the key point of this selection.

Two types of reinforcement have been selected for the composite fastener, both produced by icotec ag with Hexcel IM7 carbon fiber, the first is composed of continuous carbon fibers (CF) and the second with dedicated length short CF. This latter has been designed and manufactured on demand after primary test on continuous CF samples to explore the potential of better fastener break-up during demise.

CF/PEEK bolts and nuts are produced using a composite flow moulding technique. Such method allows the integration from continuous to short reinforcement fibers with an optimal fiber volume fraction V_f of 55%. Bolt samples material and dimensions have been selected according to the manufacturer's stock availability. Such manufacturing method induces a non-homogeneous microstructure with preferential longitudinal fiber orientation. A stainless steel (SS) A2-70, AISI 304 grade such as shown in Fig. 2, is selected as a reference material from its wide availability and its typical use for aerospace applications due to its high corrosion resistance.

Both reinforcement design microstructures have been analyzed by digital microscopy and X-ray phase-contrast imaging (XPCi) based on experimental parameters from Teixidó et al. [14], with no significant differences observed regarding fiber distribution or porosity, as shown in Fig. 3. This latter novel non-destructive evaluation technique principle revolves around an interference pattern generation that undergoes specific alterations when an object is positioned between the X-ray source and gratings. Consequently, the phase modulation leads to intensity modulation, and by analyzing such alterations in the intensity pattern with and without the sample, small and ultra-small angle scattering images can be identified. Its high sensitivity to inconsistencies within a sample at a scale smaller than the image resolution, makes it ideal for observing materials with comparable absorption and refraction characteristics but distinct microscopic internal structures, which is typically the case of fiber-reinforced polymer composite systems.

3 Testing methods

3.1 Mechanical properties evaluation

3.1.1 Tensile test

The test procedures follow ASTM D3039 and ASTM E8 to evaluate, respectively, the tensile properties of the composite and the metallic samples. A displacement rate of 2 mm/min has been selected. The load is controlled by a 100 kN MFL universal tensile machine (UTM) machine with a self-design M5 bolt holder. The sample displacement is measured by a video extensometer equipped with bilateral telecentric lens and a red back-light, as exposed in Fig. 4. The test outputs are the fracture behavior, the elastic modulus, the yield and ultimate tensile strength following ASTM D3039 chord

Fig. 2 Baseline stainless steel versus our novel CF/PEEK bolts for through-thickness insert fixture to a sandwich panel

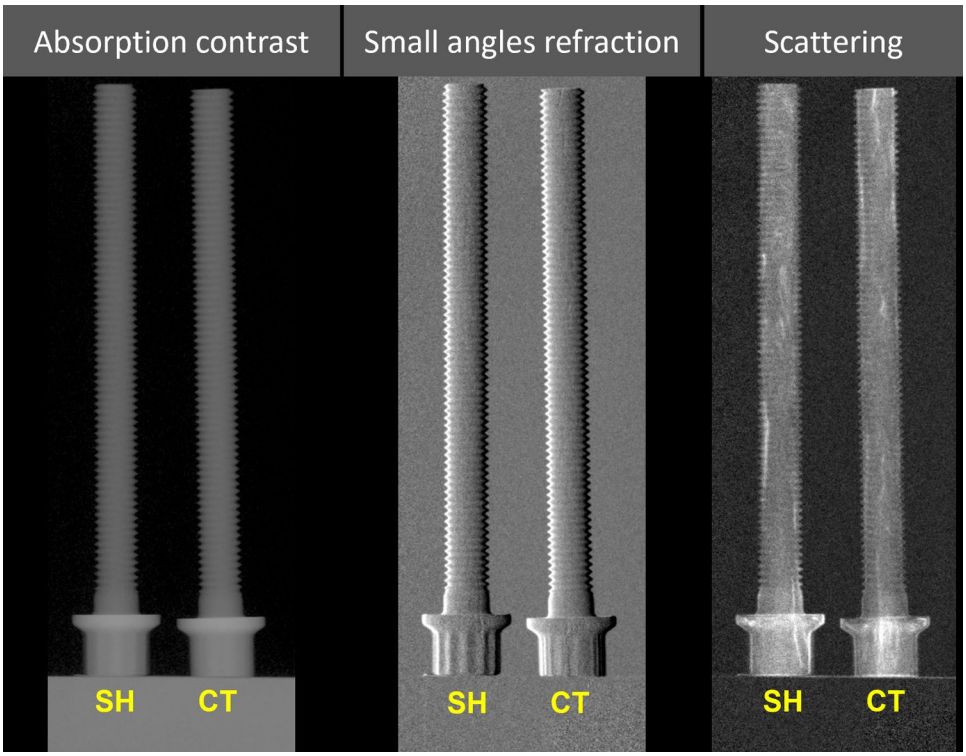

Fig. 3 Comparative analysis of continuous (CT) and short (SH) CF/PEEK samples with LPAC XPCi setup from which three type of images can be extracted. The phase scattering image showing rich microstructure information such as fiber distribution homogeneity or voids, which is particularly interesting for composite materials

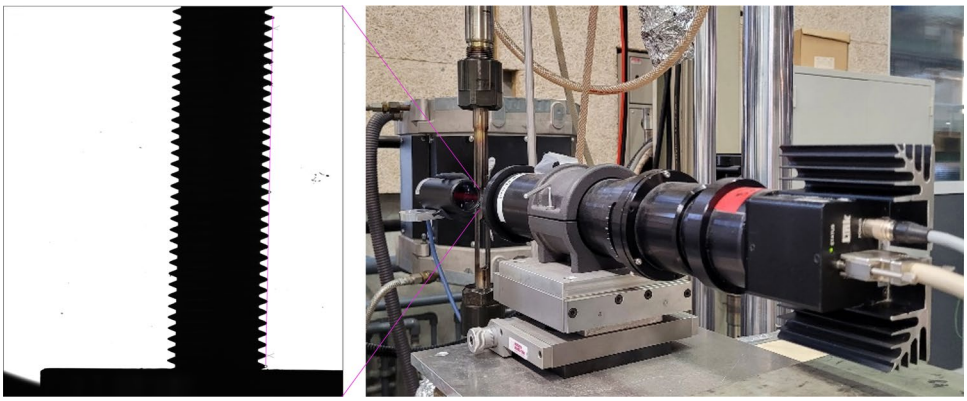

Fig. 4 Tensile test setup with the video extensometer at the forefront and the red back-light on the left. The sample is placed in between allowing a strong and clear contrast ideal for displacement measures

calculation method, where the thread stress area is calculated from the ASTM F606-21. The fasteners assembly was composed of a CF/PEEK or SS bolt with a SS nut in both cases.

3.1.2 Single shear test

The test procedure is based on ASTM F606/F606M-21 with stainless steel plates holder. The fastener assembly was composed of a CF/PEEK or SS bolt with a SS nut in both cases, and SS washers have been placed on each side of the assembly to distribute the stress as illustrated in Fig. 5. A selected preload of 2.5 kN has been applied by a respective tightening torque of 2.5 Nm and 5.1 Nm for CF/PEEK and SS samples using a dynamometric torque-wrench, then the plates are separated at a speed of 2 mm/min. In addition to force and displacement, a camera monitors possible bolt and nut rotation with respect to the holding plates.

3.1.3 Tightening capability cycling test

This test aims to evaluate the tightening cyclic preload capacity and lubrication influence on the novel short CF/PEEK bolt (same grade as indicated in Table 1). It has been performed on a dedicated setup of the Construction Laboratory from SFS Groupe Schweiz AG. It is composed of a 200 Nm drive motor mounted on a vertical drill-mill machine, a 50 Nm torque load cell and a 50 Nm/25 kN preload axial load cell. An aluminum AlMgSi grade head

Fig. 5 Single shear test setup with a CF/PEEK fastener

plate has been selected to reproduce a baseline sandwich panel aluminum insert.

The test campaign is carried out in two phases, first a single tightening cycle up to a defined preload to assess Isopropyl Alcohol (IPA) effect as tightening lubricant against unlubricated samples, five samples of each batch were tested. Then following the first phase results, a second phase consisted of a tightening cycling test of ten repetitions up to a defined preload with again five samples.

3.2 Demise evaluation

This evaluation step is based on three different tests: a thermogravimetry analysis, followed by dynamic mechanical analysis, and finishing with a static re-entry chamber.

3.2.1 Thermogravimetry analysis

A Perkin&Elmer TGA 4000 equipment was used for thermophysical measurement with machine's limits testing parameters set with a temperature sweep from 30 to 900 °C and heating rate of 40 °C/min. These settings were chosen to assess thermophysical properties under conditions as closely resembling re-entry as possible. The analysis has been performed separately under synthetic air (20%v/v O_2) and nitrogen atmosphere (N_2) with alumina crucibles and initial sample masses ranging between 10 and 15 mg. This method evaluates the mass loss of a small sample along with temperature increase, allowing the identification of the degradation onset temperature, the mass loss rate, and the residual mass as described by ASTM E1131-20.

3.2.2 Dynamic mechanical analysis

A TA Q800 analyzer equipped with a 3-point bending fixture, as displayed in Fig. 6, was selected for thermomechanical evaluation in the space mission temperature range. It allows the identification of the matrix glass and melting onset temperatures in addition to the evolution of the storage/elastic modulus with temperature.

The testing parameters were set with a temperature sweep from − 150 to 350 °C, a heating rate of 10 °C/min, and a constant 0.1% strain following ASTM D4065-20 recommendations. The CF/PEEK sample's 2 mm thickness has been selected to comply with the load cell limitations.

Table 1 Bolt samples characteristics

Material	CF/PEEK—55%V_f		Stainless steel
Density ρ	1.55 g/cm^3		7.7 g/cm^3
Emissivity (averaged along tested T)	0.79 [12]		0.69 [13]
Grade	Continuous CF	Short CF	A2-70-AISI 304
Standard	UNJF 10–32		M5
Diameter [mm]	4.7625		5
Length [mm]	50 and 55		55
Datasheet elastic modulus [GPa]	30–50 (icotec ag)	–	190–203 [10]
Datasheet ultimate tensile stress [MPa]	290 (icotec ag)	–	700 [10]
Datasheet ultimate shear stress [MPa]	349 (icotec ag)	–	490–530 [10]

There is no datasheet for short CF/PEEK as it was manufactured on request for the project

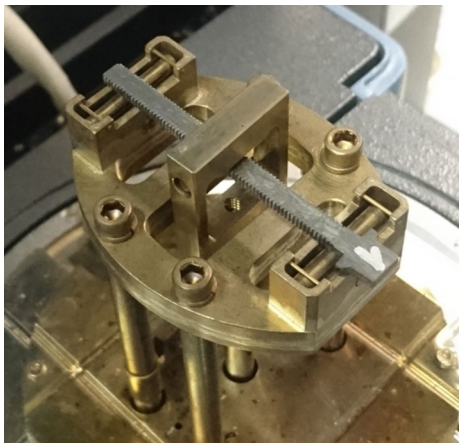

Fig. 6 DMA 3pt-bending setup with CF-PEEK sample

3.2.3 Creep static re-entry chamber

For the third demise evaluation test, a self-designed creep static re-entry chamber setup, as illustrated in Fig. 7 was used. It is based on a hydraulic MFL 100 kN tensile machine that monitors the displacement while applying a constant preload. The environmental chamber is composed of a quartz tube allowing optical test monitoring capability, a vacuum pump down to 10^{-5} mbar, and a 12 kW parabolic infrared radiative heater, capable of a 100 kW/m^2 heat flux. The applied heat flux is set to follow two specific predesigned uncontrolled re-entry temperature profiles via thermocouple control. The first is based on the Space Shuttle Mission 96 (STS-96) external temperature re-entry data [15], and the second the heating rate has been reduced by around a factor of 3 to follow a typical uncontrolled heating rate. The testing procedure is based on the ASTM D7337/D7337M and sample manufacturer recommendations, such as a creep preload of 2.9 kN.

As shown in the right image of Fig. 7, an alumina tube is placed on the bolt sample fitting the holder central spacing to act as a heat shield to simulate the fastener's real configuration where only the head/nut are exposed to the heat flux. In addition to three Type-K thermocouples, allowing multi-location temperature measurements (top, center, and bottom of the sample for example), a Canon 700D high-definition optical camera monitors the demise behavior.

From this test, mechanical and demise timing and temperature onsets can be determined in addition to tensile capability with regard to temperature and overall demise behavior.

4 Results and discussion

4.1 Mechanical performance comparative evaluation

Comparative tensile and shear stress–strain curves are provided in Fig. 8, with the material relevant properties reported in Table 2. The CF bolt design with short fibers exhibits very similar behavior as the long CF one, with less than 5% loss of tensile or shear properties compared to the baseline continuous CF composite. With such small properties' differences, it is difficult to associate the reinforcement type as the major cause, as errors from measurement techniques, such as the displacement evaluation from the video extensometer which is limited by image pixel, and equipment sensibility have been evaluated to be around a 2–4% range each. In addition, the results found for the continuous CF bolt are in good agreement with the datasheet as indicated in Table 1.

As a result, 80% and 300% improvement of the specific tensile and shear strength, respectively, can be achieved by

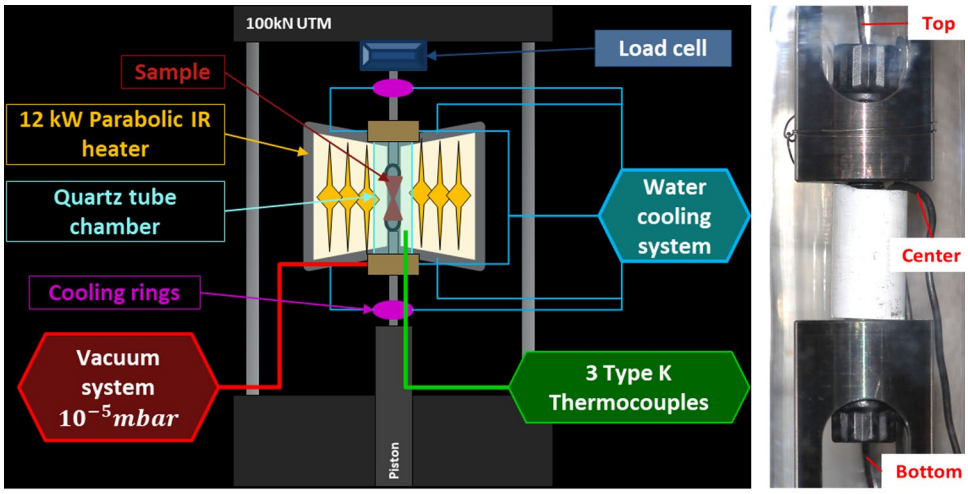

Fig. 7 **a** Self-designed static re-entry chamber illustration. **b** The bolt/nut through-thickness joint tensile creep test assembly with alumina cover and the three thermocouples' positions

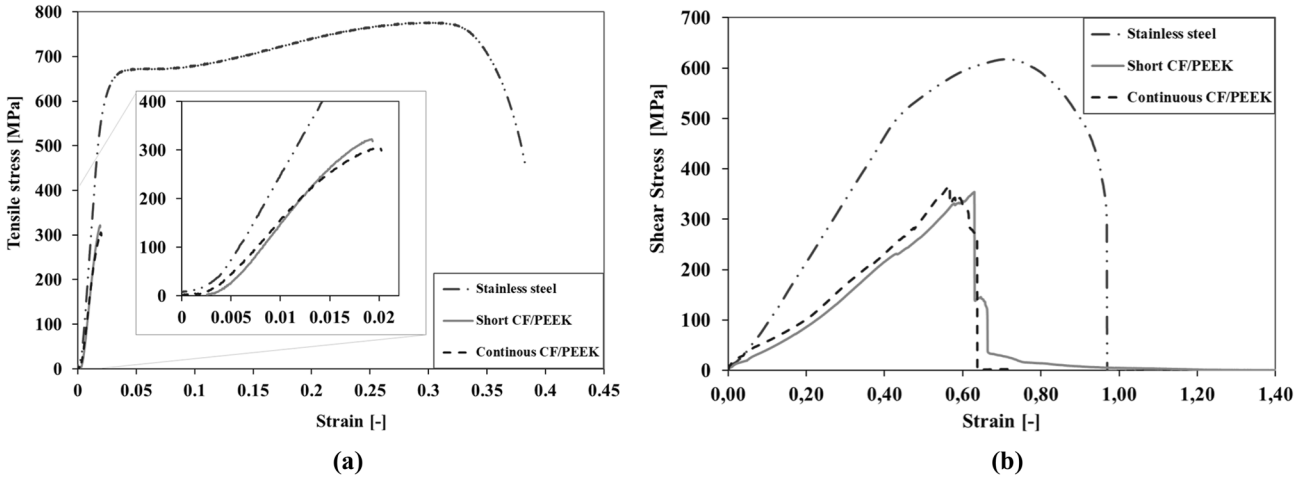

Fig. 8 Comparative **a** tensile and **b** shear stress–strain curves between SS, continuous and short CF/PEEK samples

Table 2 Summarized tensile and shear test results of the two CF/PEEK versions and the SS bolts

Material	CF/PEEK—55%V_f		Stainless steel
	Continuous CF	Short CF	
Tensile			
F_{max} [kN]	3.6 ± 0.3	3.5 ± 0.3	11.0 ± 0.1
Yield stress σ_Y [MPa]	239.0 ± 20.8	227.5 ± 15.1	520.9 ± 13.3
Max stress σ_{UTS} [MPa]	285.8 ± 21.1	276.4 ± 26.2	777.3 ± 5.4
Specific strength σ_{UTS}/ρ [MPa/kg m^{-3}]	184.4	178.3	101.0
Elastic modulus [GPa]	56.4 ± 3.6	55.2 ± 6.5	189.9 ± 16.5
Shear			
F_{max} [kN]	4.6 ± 0.1	4.5 ± 0.4	8.1 ± 0.6
Max stress τ_{USS} [MPa]	364.9 ± 2.3	350.7 ± 32.1	568.5 ± 42.2
Specific strength τ_{USS}/ρ [MPa/kg m^{-3}]	235.4	226.3	73.8

replacing stainless steel with CF/PEEK. Both composite fasteners show as expected a brittle fracture behavior. This is illustrated by their sharply ending stress–strain curves in Fig. 8, wherein comparison of SS samples shows a clear ductile fracture behavior with large plateaus and high maximum strain. If we focus more specifically on the shear failure trend, the SS samples showed an expected round ductile failure trend. Where the continuous CF/PEEK samples present sharp small multi-step failure due to the localized displacement of various continuous CF bundles within the geometry section. A behavior that is not observed for the short-reinforced version as these bundles have a finite length which act as failure initiation points without allowing additional displacement.

For the tightening capability test first phase, conducted at preloads of 2.5 kN and 2 kN, a heterogeneous outcome can be observed from the data presented in Table 3. It is characterized by closely equivalent average torque values obtained for both lubricated and unlubricated conditions. Alongside this observation, there is a notable measurement variability, particularly pronounced in relation to the loading torque. The most consistently identified lubrication effect manifests in the loading torque plateau, where a smoother and slightly reduced value is apparent as the applied rotation angle increases. From this trend, it has been decided that the second multi-cycling test phase would be performed

Table 3 Summary of the single loading cycle test results on short CF/PEEK bolt and nuts for IPA lubrication effect evaluation

Preload	2.5 kN	2 kN
Applied torque, Ma [Nm]		
Unlubricated	4.51 ± 0.50	3.76 ± 0.47
Lubricated	4.23 ± 0.93	3.87 ± 0.92
Reduction with lubrication %	−6.17%	+2.89%
Loading torque, Me [Nm]		
Unlubricated	0.47 ± 0.34	0.220 ± 0.095
Lubricated	0.27 ± 0.04	0.224 ± 0.035
Reduction with lubrication %	−41.39%	+1.82%

with lubrication. Due to samples core shear fractures with selected preload of 2.5 kN and 2 kN, a final preload of 1.5 kN allowed the test completion of the ten repetitions for each of the five samples.

Each cycle/sample application torque can be found in the graphs of Fig. 9. For the 1.5 kN preload, the application torque trend with respect to cycle number shows a clear higher torque level for the first cycle, then it increases slowly up to the fifth cycle and then stabilized with a plateau up to the last cycle. Therefore, it can be concluded that safe multiple tightening of this specific short CF/PEEK bolt design are limited to a preload of $Fn_{max} = 1.5$ kN and an application torque of Ma = 3.9 Nm.

Using digital microscopy and phase contrast X-ray imaging analysis techniques in addition to manufacturing quality control, these methods allow post-test damage evaluation such as displayed below in Fig. 10. The tightening fracture damaged area in the second bolt from the right can be clearly identified from the refraction and scattering images; whereas in contrast on the right sample, no critical damage seems to be induced by a lower preload testing, respectively, 2.5 kN vs 2 kN.

4.2 Demise relevant properties' evaluation

The three tests used for this section allow the measurement of onset temperature and timing of mechanical loosening, melting, demise/degradation of the samples, in addition to physical demise behavior observations.

The mass loss curves from Fig. 11 and reported values of Table 4, indicate that under nitrogen, the CF/PEEK degradation starts earlier in term of temperature (− 21 °C), but achieves a slightly lower maximum mass loss rate (− 15%) than under air. After 630 °C, the demise in air continues at a faster rate with temperature than under nitrogen. It can be noted that even with an identified melting temperature under air of around 335 °C from DMA results, the thermal degradation starts only around 615 °C. This earlier onset

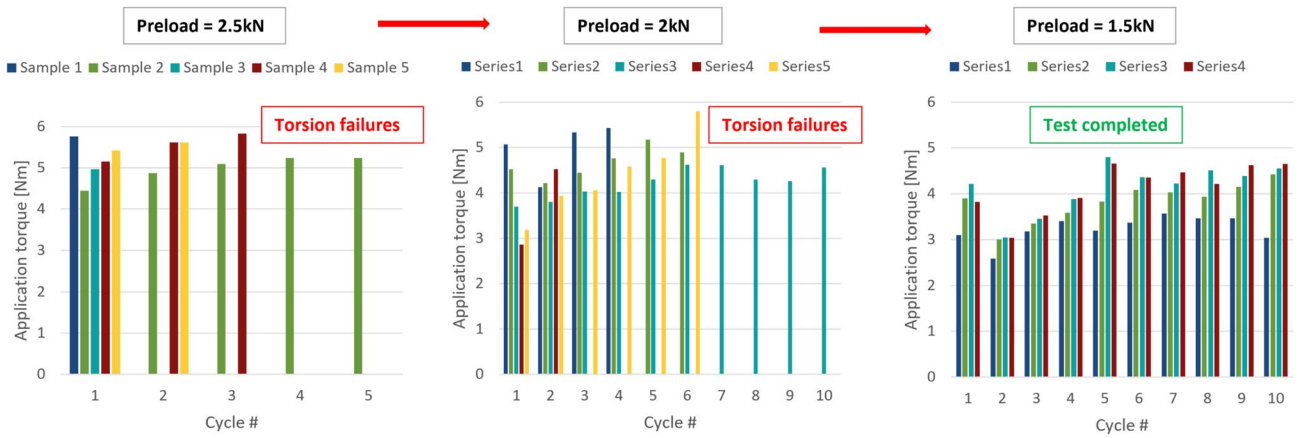

Fig. 9 Ten repetition load cycling results on short CF/PEEK bolt and nut with respective final chosen preload of 2.5 kN (left), 2 kN (middle) and 1.5 kN (right)

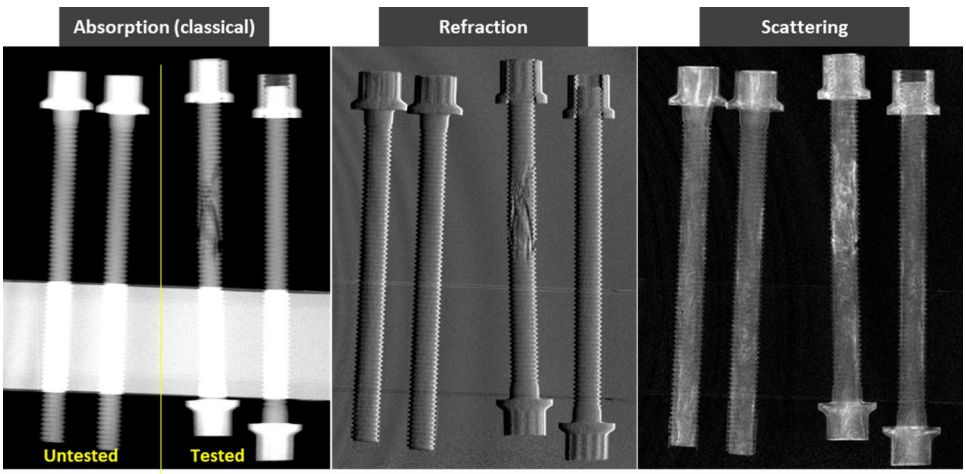

Fig. 10 XPCi post-cycling tightening test analysis on short CF/PEEK new (left pair) versus tested (right pair) bolt samples. A clear fracture can be observed in the left tested sample after three preloads cycles at 2.5 kN, against no visible damages for a recovered 2 kN sample (right). The white band on the absorption image corresponds to the PMMA sample holder

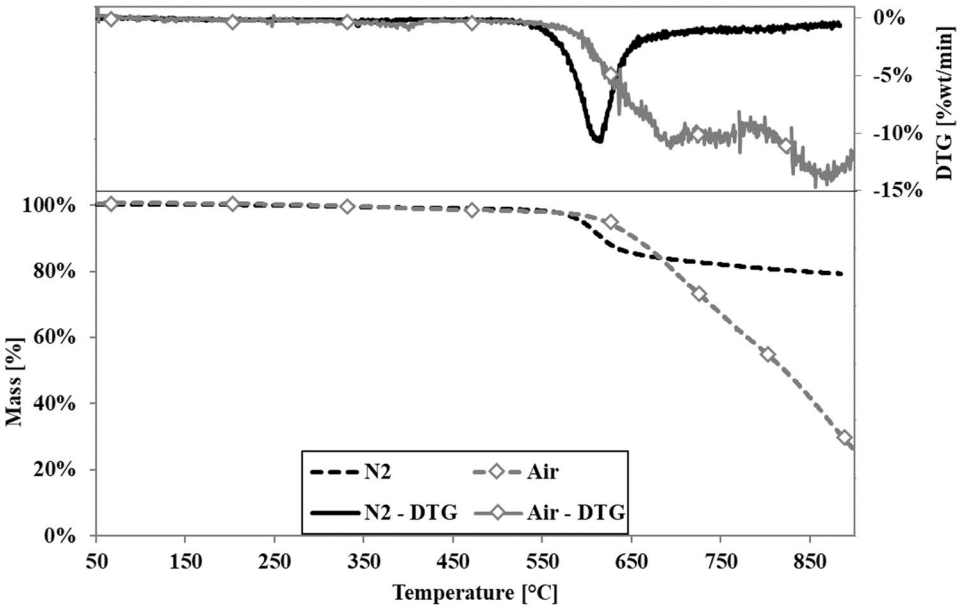

Fig. 11 TGA (bottom) and DTG (top) curves of CF/PEEK under air and nitrogen atmosphere

Table 4 TGA results summary

Environment	$T_{degradation\ onset}$ [°C]	$T_{max\ weight\ loss}$ [°C]	Max weight loss rate [%wt/min]
Air	606.7 ± 20.4	683.5 ± 114.0	− 13.2 ± 2.4
Nitrogen—N_2	585.9 ± 1.3	614.7 ± 2.4	− 11.3 ± 0.8

under a nitrogen atmosphere is attributed to the use of a high heating rate of 40 °C/min to mimic UC re-entry conditions, instead of the standard 5 °C/min. So as observed in figures 3 and 13 in the work of Ramgobin et al. [16], a higher heating rate induces a considerably significant larger shift to higher degradation onset temperature under air than under nitrogen.

In a nitrogen atmosphere, the mass loss rate significantly decreases; while in an air atmosphere, it continues steadily upon 650 °C. The oxidation process of the pyrolyzed PEEK matrix char and the CF is initiated around that point, with the clear trend difference between DTG measurements under air versus nitrogen, and reaches a near-steady state around 700 °C. The multifactorial oxidation kinetics under such conditions, lead to a high selection variability of the maximum mass loss temperature, which can be seen reported in Table 4. The non-zero mass-loss rate under nitrogen supposedly comes from a second volatilization and dehydrogenation of the residues formed during the initial decomposition stage, as it has been also observed in previous work [17, 18].

Storage modulus curves and summarized DMA data from Fig. 12 confirm that the short CF samples behave very similarly as the continuous ones, with similar glass temperature, melting temperature and storage modulus. Optimal mechanical properties of CF/PEEK bolt can be maintained while operating between − 150 and 118 °C. Melting starts around 335 °C, which is significantly advantageous regarding demisability as compared to respectively 1380 °C or 1660 °C of the SS or Ti–6Al–4V for a bolt joint system, as it should lose its assembly capability close to this specific point.

From the third demise-oriented test, CF/PEEK mechanical and demise timing and temperature onsets have been characterized under two relevant static re-entry conditions, named UC and STS-96 as presented in Fig. 13, and where the main characteristics points are reported in Table 5. From the top graph of Fig. 13, it can be observed that axial displacement and the top surface temperature evolutions along the applied UC temperature profile are very similar between the two CF/PEEK samples, although the fracture types and recovered samples present disparities. The continuous CF samples mostly showed a brittle core fracture under both heating rate conditions, where for the short CF ones, the trend was different between the two testing conditions. Under STS-96 (high heating rate), they all presented a thread stripping failure, against a mix of both for the tests under UC (low heating rate) conditions. Concerning the thermomechanical aspect, continuous CF design presents an earlier loosening with lower onsets temperatures, respectively, − 40 °C and − 51 °C when compared to the short CF. A trend linked to the short reinforcement samples showing a 45% higher failure strain. Therefore, differences that seems to be directly linked to the specific reinforcement length.

Regarding now the heating rate influence, an expected fracture temperature delay under a higher heating rate is verified, with a difference around 24 °C for continuous CF and 35 °C for the short CF. But an opposite trend is observed in the case of the demise onset temperature, where a respective

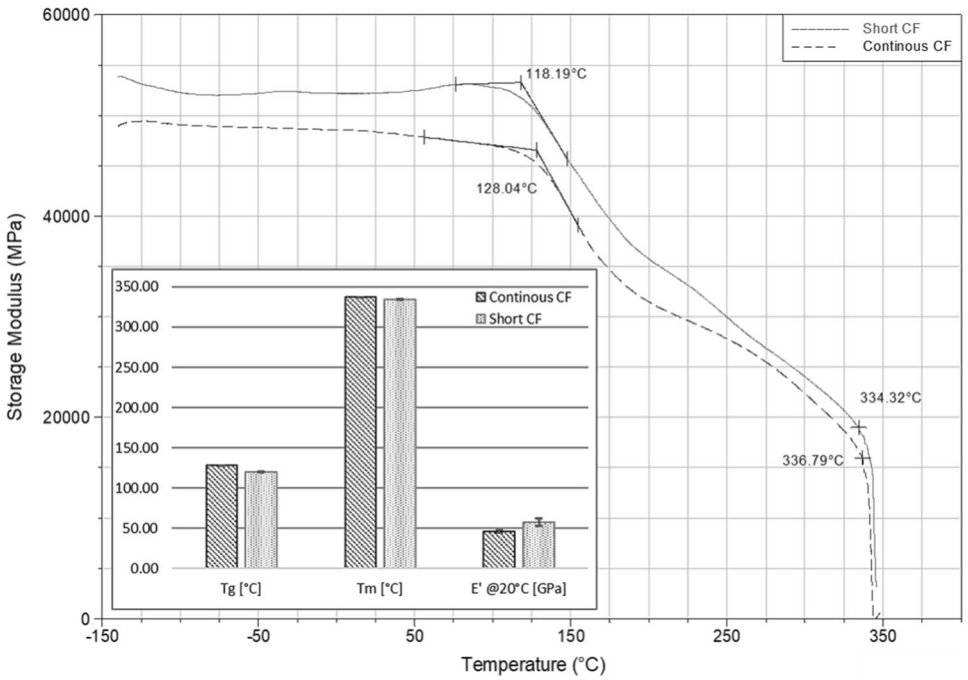

Fig. 12 DMA curves of the storage modulus evaluation from − 150 to 350 °C of continuous versus short CF/PEEK samples. In the bottom left, DMA results summary

reduction of − 71 °C and − 8 °C from average values is measured with a higher heating rate. The most probable cause from this abnormal trend might come from the setup difficulty to fit exactly the set temperature profile and thus leading in high variability in the high temperature range, in which the demise is happening. In addition, temperature plateaus are observed for both composite sample types before 200 s under STS-96 test conditions, closely aligning with the visual observation of the matrix demise onset. This distinct temperature behavior is not observed during the UC reentry characterized by a lower heating rate regime. Hence, it signifies that under such elevated heating rate conditions, the matrix's endothermic pyrolysis reaction and outgassing substantially diminish the incoming heat flux.

A critical difference of the recovered samples physical performance has been observed and led to the identification of the short CF as an optimal demisable bolt design, this can be observed by the remaining assembly capability after test in Fig. 14. The observed optimal weak pull-out separation behavior with short CF fasteners, where complete separation of the holder was achieved without additional break-up forces, indicates that above the demise temperature such design allows a complete release of the joining system, such as external sandwich panels for example.

As observed under the STS-96 conditions and displayed in Table 5, by switching from SS to such CF/PEEK composite alternative, the mechanical loosening onset can be reduced by 500 °C, besides the reduction of at least 380 °C for the demise onset, since no demise behavior has been observed for the SS within this testing range. Therefore, a drastically improved potential for the overall spacecraft demise process can be demonstrated by a much earlier break-up.

5 conclusion

As part of a general mitigation plan to deal with surviving re-entering space debris threat, the exposed design for demise approach aims to achieve a safe and sustainable space environment by playing with material substitution and spacecraft break-up sequence.

To determine the viability and demise efficiency of a novel fastener material assembly for spacecraft panels, a comparative evaluation has been performed between two CF/PEEK designs and a stainless steel reference.An optimal composite bolt design such as represented in Fig. 15, made of short CF reinforcement in a PEEK matrix, has been characterized and compared to a continuous CF baseline version by microstructure analysis, thermomechanical and tensile testing. The short fiber design does not show any significant loss of mechanical properties at ambient temperature or within the space qualification temperature range of ± 120 °C.

The demise evaluation by static re-entry chamber under two deorbit-like conditions allowed the identification of heating rate influence on the surface temperature. Where it was observed that the preeminent processes governing PEEK demise, pyrolysis and outgassing, exhibited a significant effect on the surface temperature. Specifically, when subjected to the highest heating rate, these processes yielded a substantial reduction in surface temperature, diverging

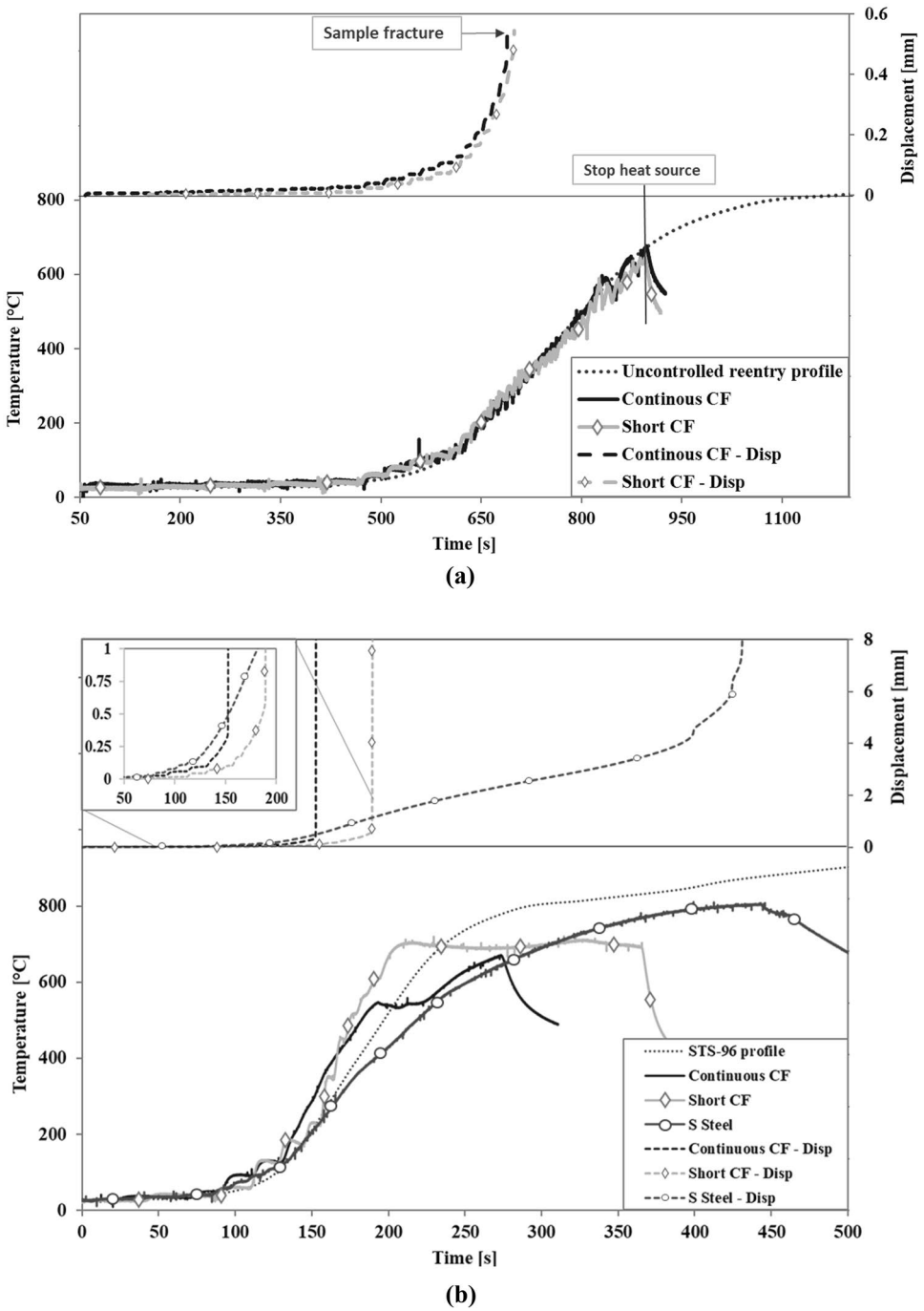

Fig. 13 Sample temperature and displacement of continuous and short CF/PEEK samples under the two different re-entry profiles, respectively **a** UC on the top and **b** STS-96 on the bottom. In this latter a tested SS sample is additionally displayed

clearly from the anticipated trend observed at lower heating rate.

This study therefore highlights its ideal complete failure/separation after a short exposure to high heat flux, a point around 10 min along an uncontrolled re-entry-like flight path or with a surface temperature higher than 500 °C. An added advantage of this bolted-joint system lies in its familiarity and extensive utilization as an assembly technique in the space industry sector. This inherent recognition and application should streamline the acceptance and implementation procedures, setting it apart from other existing innovative composite designs. Moreover, composites present a large specific strength improvement as compared to the re-entry resistant stainless steel design, although more bolts will be needed to sustain an equivalent load as compared to stainless steel bolts. And where such technology limitations compared to baseline metallic bolt fasteners, a re-design of insert dimensions such as more attachment points or larger diameter would be required. Although CF and PEEK components have demonstrated flight-proven reliability [19],

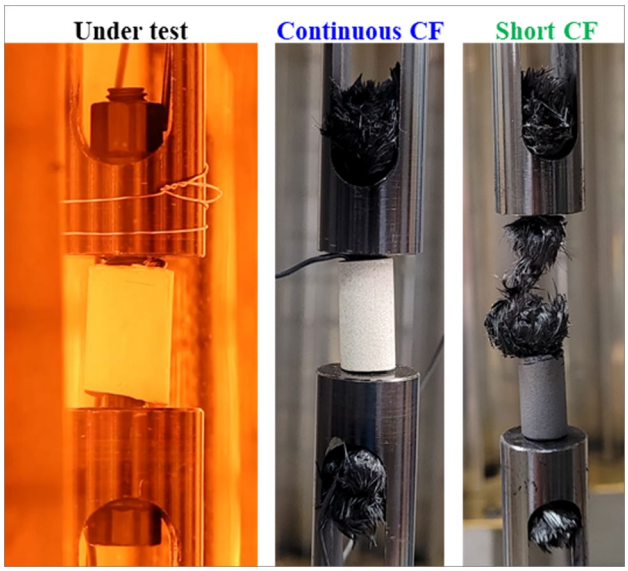

Fig. 14 Left, CF/PEEK sample under static re-entry test. Right, recovered continuous and short CF/PEEK samples from static re-entry test, with a complete fastener separation in the case of the short CF bolt

like any composite system, they might still exhibit higher variability in sample quality compared to baseline materials.

The project's next phase will be to focus on specific space qualification testing such as thermal cycling creep testing and vibration resistance. In addition to a complete benchmark sandwich panel assembly validation test within a high-fidelity plasma wind tunnel (PWT) facility. Furthermore and aside from the technical points, additional work will be necessary to assess the overall environmental impact of such material substitution and especially the understudied effects on the upper-atmosphere regions. Based on recent studies evaluating the global environmental impact of the space sector, dedicated life cycle analysis (LCA) research highlights the need to address the knowledge gap regarding the environmental effects of objects re-entering Earth's atmosphere [20–22].

As a final goal, this multi-collaborative project aims to achieve a TRL6 so this technology can be implementable on a S/C such as ClearSpace-One, and thus paving the way for a more safe and sustainable space, aligning with ESA's recently published Zero Debris policy [23].

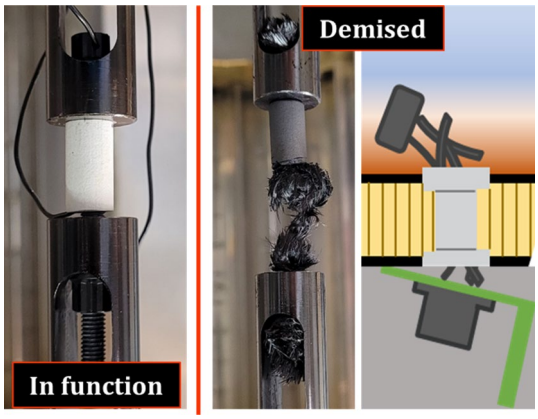

Fig. 15 Illustration of the ideal short CF/PEEK fastener demise within an external sandwich panel

Table 5 Static re-entry creep test results summary for through-thickness bolted joint system under typical re-entry heating profiles

Test condition	UC re-entry		STS-96		
Material	CF/PEEK		CF/PEEK		SS
	Continuous	Short	Continuous	Short	
Fracture onset					
Time [s]	635 ± 45	666 ± 29	154 ± 4	160 ± 8	432
Temperature [°C]	212.0 ± 38.0	252.5 ± 37.5	235.8 ± 27.0	287.0 ± 29.1	802
Strain [–]	0.84 ± 0.41	1.3 ± 0.03%	1.06 ± 0.14%	1.56 ± 0.07%	17.83%
Demise onset					
Time [s]	805 ± 2	758 ± 18	193 ± 11	186 ± 5	No demise up to 820 °C (test termination)
Temperature [°C]	502.1 ± 1.2	401.0 ± 19.0	430.8 ± 16	393.0 ± 11	

Acknowledgements This work is supported by ESA through an NPI program #4000129740/20/NL/MH/hm. The authors also acknowledge all the project partners, Beyond Gravity AG, icotec ag, IRS, Belstead Research, ClearSpace and Bcomp for their active collaborative and financial support. We also thank Dr.Valentin Rougier for the X-ray images acquisition and Raphael Charvet for his crucial help on technical aspects of the testing equipment.

Funding Open access funding provided by EPFL Lausanne.

Data availability The datasets generated and analyzed during the current study are available from the corresponding author on reasonable request.

Declarations

Conflict of interest The authors declare that they have no conflicts of interest.

References

1. Chronology of Space Launches—Gunter's Space Page. https://space.skyrocket.de/directories/chronology.htm. Accessed 22 Aug 2023
2. ESA, ESTEC: DIVE—guidelines for analysing and testing the demise of man made space objects during re-entry. https://sdup.esoc.esa.int/documents/download/Design-for-Demise-Verification-Guidelines-v1.pdf (2021)
3. Pagan, A., et al.: Characterisation of demisable materials through plasma wind tunnel testing. Submitted to "8th European Symposium on Aerothermodynamics for Space Vehicles, Lisbon-Portugal". https://www.researchgate.net/profile/Adam-Pagan/publication/280085112_Characterisation_of_Demisable_Materials_through_Plasma_Wind_Tunnel_Testing/links/55a77f9108aea2222c745bb3/Characterisation-of-Demisable-Materials-through-Plasma-Wind-Tunnel-Testing.pdf (2015)
4. ESA's re-entry predictions. https://reentry.esoc.esa.int/home/recovereddebris. Accessed 28 May 2022
5. Pagan, A., et al.: Experimental investigation of material demisability in uncontrolled earth re-entries. Submitted to "31st International Symposium on Space Technology and Science, *Matsuyama-Japan*". https://www.researchgate.net/publication/318360979_Experimental_Investigation_of_Material_Demisability_in_Uncontrolled_Earth_Re-entries (2017)
6. Heinrich, S., Martin, J., Pouzin, J.: Satellite design for demise thermal characterisation in early re-entry for dismantlement mechanisms. Acta Astronaut. **158**, 161–171 (2019). https://doi.org/10.1016/j.actaastro.2018.03.021
7. Fittock—new design for demise technology concepts for stru.pdf. https://indico.esa.int/event/234/contributions/4038/attachments/3019/3641/2018_CSID_Fittock_OHB_D4DBB_Tech_Concepts_v0-2.pdf. Accessed 23 Oct 2023
8. Grassi, et al.: ITI, innovation triangle initiative—demisable jo.pdf. https://indico.esa.int/event/234/contributions/3923/attachments/3089/3797/2018CSID_LGrassi_DemisableJoint.pdf (2017). Accessed 23 Oct 2023
9. Patzwald, J.: High altitude break-up concepts with additively manufactured CF-PEEK. In: Presented at The Cleans Space Industry Days 2021, ESTEC, Sept. 22, 2021. https://indico.esa.int/event/321/contributions/6386/attachments/4354/6570/Presentation%2520Patzwald%2520-%2520ESA%2520Clean%2520Space%2520Days.pdf. Accessed 26 Oct 2023
10. Online materials information resource—MatWeb. https://www.matweb.com/. Accessed 28 May 2022
11. Nakamura, T., Nakamura, H., Fujita, O., Noguchi, T., Imagawa, K.: The space exposure experiment of PEEK sheets under tensile stress. JSME J. Int. J. Ser. A **47**(3), 365–370 (2004). https://doi.org/10.1299/jsmea.47.365
12. Pagan, A., Herdrich, G.: Key parameters governing the ground risk from reentering pressure vessel debris. J. Space Saf. Eng. **9**, 189–200 (2022). https://doi.org/10.1016/j.jsse.2022.04.002
13. Pagan, A.S., Massuti-Ballester, B., Herdrich, G., Merrifield, J.A., Beck, J.C., Liedtke, V.: Developing an experimental procedure towards a standardised testing of aerospace material demisability. Presented at Clean Space Industry Days, 23–26 April 2016. https://indico.esa.int/event/128/attachments/736/897/04_IRS_FGE_BRL_AAC_Presentation_CoDM_2016-05-25.pdf (2016)
14. Teixidó, H., Caglar, B., Revol, V., Michaud, V.: In-operando dynamic visualization of flow through porous preforms based on X-ray phase contrast imaging. Compos. Part A Appl. Sci. Manuf. **149**, 1065601 (2021). https://doi.org/10.1016/j.compositesa.2021.106560
15. Blanchard, R., et al.: Infrared sensing aeroheating flight experiment: STS-96 flight results. J. Spacecr. Rocket. **38**, 465–472 (2001). https://doi.org/10.2514/2.3713
16. Ramgobin, A., Fontaine, G., Bourbigot, S.: A case study of polyetheretherketone (II): playing with oxygen concentration and modeling thermal decomposition of a high-performance material. Polymers (Basel) **12**(7), 1577 (2020). https://doi.org/10.3390/polym12071577
17. Patel, P., et al.: Investigation of the thermal decomposition and flammability of PEEK and its carbon and glass-fibre composites. Polym. Degrad. Stab. **96**(1), 12–22 (2011). https://doi.org/10.1016/j.polymdegradstab.2010.11.009
18. Fontaine, P., Weiss-Hortala, E., Botaro, V., Paiva, J.M.F., Soudais, Y.: Impact of atmosphere on recovered carbon fibers from poly ether ether ketone (PEEK) based composites during thermoconversion. Waste Biomass Valor. **12**(12), 6389–6402 (2021). https://doi.org/10.1007/s12649-021-01445-7
19. Caldwell, S.: NASA-6.0 structures, materials, and mechanisms. NASA. http://www.nasa.gov/smallsat-institute/sst-soa/structures-materials-and-mechanisms. Accessed 01 Jul 2023
20. Udriot, M., Treyer, K., David, E., Bühler, O., Etesi, L., Girardin, V.: Rapid life cycle assessment software for future space transportation vehicles' design—the assessment and comparison tool. In: Presented at the Aerospace Europe Conference 2023—10th EUCASS–9th CEAS, EPFL, Lausanne, June 2023, p. 15. https://doi.org/10.13009/EUCASS2023-015
21. Hellmich, S., Udriot, M., Yap, X.-S., David, E., Looten, A.A.: Sustainable space hub at EPFL: a review of ongoing research projects. In: Presented at the Aerospace Europe Conference 2023—10th EUCASS–9th CEAS, June 2023, p. 15. https://doi.org/10.13009/EUCASS2023-016
22. Delaval, J.: On the atmospheric impact of spacecraft demise upon reentry—the clean space blog. On the atmospheric impact of spacecraft demise upon reentry. https://www.blogs.esa.int/

cleanspace/2022/08/11/on-the-atmospheric-impact-of-spacecraft-demise-upon-reentry/. Accessed 23 Oct 2023
23. ESA Space Debris Mitigation Policy, 3 November 2023, ESA-ADMIN-IPOL-2023-1-Space-Debris-Mitigation-Policy-Final.pdf'. Accessed: 12 Dec 2023. https://technology.esa.int/upload/media/ESAADMIN-IPOL-2023-1-Space-Debris-Mitigation-Policy-Final.pdf